Special Symposium Issue 5

Proceedings of the Thirteenth Symposium on Thermophysical Properties

In Honor of Ared Cezairliyan (1934–1997)

Edited by

W. M. Haynes
National Institute of Standards and Technology
Boulder, Colorado, U.S.A.

and

R. A. Overfelt
Auburn University
Auburn, Alabama, U.S.A.

Held at

University of Colorado
Boulder, Colorado, U.S.A.
June 22–27, 1997

Organized by

National Institute of Standards and Technology
and
Committee on Thermophysical Properties
Heat Transfer Division
American Society of Mechanical Engineers

Sponsored by

Physical and Chemical Properties Division
Chemical Science and Technology Laboratory
National Institute of Standards and Technology

Symposium Chairs:

W. M. Haynes, *NIST*
R. A. Overfelt, *Auburn University*

Symposium Secretary:

B. A. Stevenson, *NIST*

Symposium CD-ROM Editor and Webmaster:

G. R. Hardin, *NIST*

Special Session Organizers:

Properties of Alternative Refrigerants	M. O. McLinden, *NIST*
Properties for Chemical Process Design	R. F. Kayser, *NIST*
Properties of Aqueous Systems	A. H. Harvey, *NIST*
Properties for Metallurgical Process Design	R. A. Overfelt, *Auburn University*
Properties of Polymers and Polymer Solutions	C. C. Han, *NIST*
Properties of Thin Films and Coatings	D. G. Cahill, *University of Illinois* W. P. Allen, *United Technologies Research Center* A. Feldman, *NIST*
Critical Behavior	M. A. Anisimov, *University of Maryland*
Molecular Simulation	R. D. Mountain, *NIST*
Subsecond Thermophysics	A. Cezairliyan, *NIST*
Structure of Fluids	H. J. M. Hanley, *NIST*
Optical Techniques	R. W. Gammon, *University of Maryland*
Laser Photothermal Techniques	A. Mandelis, *University of Toronto*
Acoustic Techniques	M. R. Moldover, *NIST*
Wetting and Interfaces	J. O. Indekeu, *Katholieke Universiteit Leuven*
Properties of Supercritical Fluids	T. J. Bruno, *NIST* J. M. H. Levelt Sengers, *NIST*
Databases and Data Correlation	D. G. Friend, *NIST* M. L. Huber, *NIST*
Properties in Low Gravity	R. F. Berg, *NIST*
Properties of Natural Gas Systems	J. W. Magee, *NIST* W. M. Haynes, *NIST*

International Journal of Thermophysics, Vol. 20, No. 1, 1999

Stochastic Thermal-Diffusion Forced Rayleigh Scattering[1]

R. Schäfer,[2] A. Becker,[2] and W. Köhler[2, 3, 4]

The holographic grating technique of thermal-diffusion forced Rayleigh scattering (TDFRS) utilizes the Ludwig–Soret effect to induce a concentration modulation within a binary liquid. The signal generation is described in terms of a linear response formalism, and the memory function for the concentration mode $g(t)$ and its Fourier transform, the diffusion susceptibility, are measured by means of pseudostochastic random binary sequences with flat power spectra in combination with fast Fourier transform and correlation techniques. For polydisperse polymer solutions the individual modes contribute proportional to their concentration to $g(t)$, contrary to photon-correlation spectroscopy, where the correlation function is dominated by the high molar mass components. Other advantages of stochastic TDFRS are time-scale delocalization of dust spikes and frequency multiplexing. Measurements are reported on monodisperse and bimodal polystyrene in toluene.

KEY WORDS: diffusion; forced Rayleigh scattering; Fourier transform; Ludwig–Soret effect; polymer solutions; stochastic excitation; thermal diffusion.

1. INTRODUCTION

A holographic interference grating written into a binary liquid, e.g., a polymer solution, gives rise to a secondary concentration grating driven by the Ludwig–Soret effect, also termed thermal diffusion [1–3]. From such thermal-diffusion forced Rayleigh scattering (TDFRS) experiments, various transport coefficients, such as the thermal diffusivity, the mutual diffusion coefficient, the thermal diffusion coefficient, and the Soret coefficient, can be determined in a very direct way. Due to the micrometer

[1] Invited paper presented at the Thirteenth Symposium on Thermophysical Properties, June 22–27, 1997, Boulder, Colorado, U.S.A.

[2] Max-Planck-Institut für Polymerforschung, Postfach 3148, D-55021 Mainz, Germany.

[3] To whom correspondence should be addressed.

[4] Current address: Physikalisches Institut, Universität Bayreuth, D-95440 Bayreuth, Germany.

0195-928X/99/0100-0001$16.00/0

diffusion length, the corresponding subsecond diffusion times, and the very subtle perturbations of the sample, many problems associated with long-term stability in traditional diffusion cell experiments disappear.

With respect to the measurement of center-of-mass diffusion, there exist several similarities between TDFRS and photon-correlation spectroscopy (PCS), but also significant differences. PCS relies on thermodynamic concentration fluctuations. In dilute polymer solutions the scattering, which is proportional to the molar mass, is dominated by the high-molar mass components, and a few heavy particles can completely mask low molar mass contributions.

TDFRS, on the other hand, allows for a coherent excitation with a single, well-defined q-vector. Since thermal diffusion is driven by the applied temperature grating, there is considerable freedom in the selection of the excitation time pattern, and periodic amplitude modulation has been proposed in the literature [4].

It has been shown that TDFRS can be employed for polydispersity analysis of dilute polymer solutions. The memory or the linear response function, which fully characterizes a linear system, is of particular interest because of the even concentration proportional statistical weights of the different molar mass components [5]. Simple attempts to measure the memory function directly by means of short excitation pulses suffer, however, from poor signal-to-noise ratios due to the low spectral power density of the excitation. Measurements with finite length pulses yield good signal-to-noise ratios, but only the convolution of the memory function with the excitation. Due to "holes" in the spectrum, a simple deconvolution is not possible.

In the following it is shown how pseudostochastic random binary sequences together with fast Fourier transform and correlation techniques can be employed to provide excitations with approximately white power spectra and a high spectral power density for the measurement of the linear response function of the concentration mode. Not all random binary sequences, however, fulfil the requirement of a flat power spectrum. Excitations with deconvolutable random binary sequences may also be viewed as spectroscopic experiments in the frequency domain with frequency multiplexing, which yield the complex diffusion susceptibility, defined as the Fourier transform of the linear response function.

2. THEORY

2.1. TDFRS Signal Generation

In the following the concept of TDFRS is outlined in a compact notation to provide the fundamental equations needed for the main part of this

paper. For a more detailed discussion of the phenomenological model and the experimental setup, the reader is referred to the literature [1–8].

For a description of the Ludwig–Soret effect in a binary liquid, an extension of Fick's second law of diffusion is employed to calculate the temporal and spatial evolution of the concentration $c(x, t)$, measured in weight fractions, under the boundary conditions imposed by the experiment:

$$\frac{\partial c}{\partial t} = D\,\Delta c + D_T c(1-c)\,\Delta T \tag{1}$$

$T(x, t)$ is the time-dependent temperature distribution, and D is the translational and D_T the thermal-diffusion coefficient. For TDFRS, $T(x, t)$ is obtained from the heat equation with the energy absorbed from the optical interference grating $I(x, t) = I_0 + I_q e^{iqx}$ as the source term:

$$\frac{\partial T}{\partial t} = D_{th}\,\Delta T + \frac{\alpha}{\rho c_p}(I_0 + I_q e^{iqx}) \tag{2}$$

Because of the underlying symmetry of the holographic experiment, a one-dimensional description has been adopted, with the x-axis defined by the grating vector $q = 4\pi\lambda^{-1}\sin\,\theta/2$. θ is the angle between the two writing beams, D_{th} is the thermal diffusivity, α is the absorption coefficient, ρ is the density, and c_p is the specific heat at constant pressure. From Eq. (2) the time-dependent temperature distribution

$$T(x, t) = T_q(t)\, e^{iqx} \tag{3}$$

with

$$T_q(t) = \frac{\alpha}{\rho c_p} \int_{-\infty}^{t} dt'\, I_q(t')\, e^{-(t-t')/\tau_{th}} \tag{4}$$

is obtained, neglecting spatially constant terms. $\tau_{th} = (D_{th} q^2)^{-1}$ is the heat diffusion time constant. Knowing $T(x, t)$, the time dependent concentration distribution is obtained from Eq. (1):

$$c(x, t) = c_0 + c_q(t)\, e^{iqx} \tag{5}$$

with

$$c_q(t) = -q^2 D_T c_0(1-c_0) \int_{-\infty}^{t} dt'\, T_q(t')\, e^{-(t-t')/\tau} \tag{6}$$

$\tau = (Dq^2)^{-1}$ is the mass diffusion time constant. Since the concentration changes are generally very subtle, the approximation $c_0 \approx c$ is used in the following.

Both c and T couple to the refractive index n, resulting in a phase grating

$$n(x, t) - n_0 = n_q(t)\, e^{iqx} = \left[\left(\frac{\partial n}{\partial T} \right)_{c, p} T_q(t) + \left(\frac{\partial n}{\partial c} \right)_{T, p} c_q(t) \right] e^{iqx} \tag{7}$$

which is read by Bragg diffraction of a readout beam.

The heterodyne diffraction efficiency $\zeta_{het}(t)$, which is proportional to the refractive index modulation depth $n_q(t)$, is obtained after normalization to the signal generated by the temperature grating alone:

$$\zeta_{het}(t) = \left[\tau_{th} \frac{\alpha}{\rho c_p} I_0 \right]^{-1} \int_{-\infty}^{t} dt'\, g(t - t')\, T_q(t') \tag{8}$$

The memory or linear response function $g(t)$ is[4]

$$g(t) = \begin{cases} \delta(t) - \left(\dfrac{\partial n}{\partial c} \right)_{p, T} \left(\dfrac{\partial n}{\partial T} \right)_{p, c}^{-1} q^2 D_T c(1 - c)\, e^{-t/\tau}, & t \geqslant 0 \\ 0, & t < 0 \end{cases} \tag{9}$$

Dilute solutions of polydisperse polymers, which cannot be described by a single diffusive mode, are of particular interest. In this case Eq. (9) must be replaced by a sum over all species k present in the sample:

$$g(t) = \sum_k g_k(t) = \delta(t) + \sum_k a_k e^{-t/\tau_k} \tag{10}$$

$$a_k = -q^2 \left(\frac{\partial n}{\partial T} \right)_{p, c}^{-1} \left(\frac{\partial n}{\partial c_k} \right)_{p, T, c_{l \neq k}} D_{T, k} c_k \tag{11}$$

Here the dilute solution approximation $c(1 - c) \approx c$ has been made.

At least in the case of dilute solutions of high polymers, there is a time scale separation of more than three decades between the heat and the concentration mode, and for experiments on the time scale of the concentration mode, the temperature grating almost instantaneously follows the

[4] Contrary to $G(t)$ used in previous publications, $g(t)$ has been chosen for a more consistent notation.

optical one. Furthermore, $(\partial n/\partial c_k)_{p,T}$ and D_T are approximately independent of molar mass [9], which reduces the molar mass dependence of a_k to the concentration c_k.

Generally, an experiment measures a convolution of the memory function of the concentration mode, $g(t)$, with the time dependent temperature excitation $T_q(t)$. A straightforward experiment consists of a long excitation pulse of finite length $\tau_p \gg \tau_k$ and constant amplitude. For polydisperse polymer solutions, this results in a multiexponential decay function with statistical weights $a_k\tau_k$ for the kth mode.

Ideally, the memory function $g(t)$, which contains all information that can be learned from a linear experiment, would be measured directly. In the most simple case this is accomplished by shortening the excitation pulse to $\tau_p \ll \tau_k$, where a multiexponential decay function with statistical weights proportional to a_k or, within above approximations, proportional to c_k is obtained [5].

It is of interest to compare heterodyne TDFRS with the electric field autocorrelation function as measured by PCS, the most widely applied technique for the measurement of diffusion coefficients. With a scaling relation $D \propto M^{-b}$, $b \leqslant 1$, for the molar mass dependence of the diffusion coefficient, the statistical weights for the multiexponential decay functions are $c_k M_k^{\alpha}$, where α is characteristic for the experiment [5]. For TDFRS, with short pulses, $\alpha = 0$; with long excitation pulses, $\alpha = b$ is found. The change of the average rate $\langle \Gamma \rangle = \langle \tau^{-1} \rangle$ as a function of exposure time is shown in Fig. 1 for a polydisperse sample. For PCS, $\alpha = 1$, resulting in a strong overestimation of the high-molar mass components in the PCS autocorrelation function.

2.2. Measurement of the Memory Function

The problem when measuring $g(t)$ directly by employing short exposure times is obvious from the vanishing signal amplitudes in the insert in Fig. 1, resulting in poor signal-to-noise ratios. The alternative of a straightforward deconvolution of a measurement with a finite pulse length is also not feasible due to holes in the power spectrum of the excitation.

A rather elegant way to measure the response function of a linear system emerged with the availability of inexpensive fast digital-computer hardware in combination with fast Fourier transform and correlation algorithms. The basic idea is to use a deconvolutable excitation with a flat, e.g., white, power spectrum of high spectral power density in combination with tailored deconvolution or correlation techniques. Such excitations can be realized by means of suitable pseudostochastic binary noise sequences.

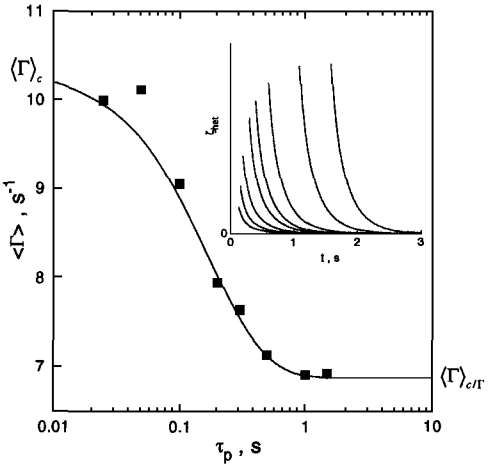

Fig. 1. Exposure time dependence of the average rate $\langle \Gamma \rangle$ for a mixture of polystyrene with $M = 48$ and $M = 556$ kg · mol^{-1} at equal concentrations of 0.0029 weight fractions. Exposure ranges from $t = 0$ up to the start of the respective decay curve. The data are taken from Ref. 5.

A special variant of such sequences, maximum length binary sequences (MLBS) [10], has been used successfully for Hadamard–NMR spectroscopy [11].

2.2.1. Fundamental Equations

Before turning to the actual experiment, some general features of linear systems, as far as they pertain to TDFRS, will briefly be summarized in a problem-independent notation. Later, the respective quantities will be mapped to the TDFRS experiment. The convention obeyed is as follows.

Signals are continuous functions in the time domain and denoted in lower case with the argument in parentheses, e.g., $x(t)$. Sampling at constant intervals Δt produces a discrete approximation $x[n]$ to the continuous signal, which is only defined at times $t = n\,\Delta t$, $n = 0, 1, 2, \ldots$. Square brackets are used for the arguments of discrete functions. The Fourier transform establishes the connection between the time and frequency domains [12]:

$$x(t) = \frac{1}{2\pi} \int_{-\infty}^{\infty} d\omega\, X(\omega)\, e^{i\omega t} \tag{12}$$

$$X(\omega) = \int_{-\infty}^{\infty} dt\, x(t)\, e^{-i\omega t} \tag{13}$$

Frequency domain functions are denoted by capital letters. Of importance for the TDFRS experiment is the discrete Fourier transform of an array of N data points within a period of $N\,\Delta t$:

$$x[n] = \frac{1}{N} \sum_{k=0}^{N-1} X[k]\, e^{2\pi i n k/N} \tag{14}$$

$$X[k] = \sum_{n=0}^{N-1} x[n]\, e^{-2\pi i n k/N} \tag{15}$$

The connection with the frequency scale is given by

$$\omega_k = \frac{2\pi k}{N\,\Delta t} \tag{16}$$

The response $y(t)$ of a linear system to an excitation $x(t)$ is a convolution of $x(t)$ with the response function $h(t)$:

$$y(t) = x(t) * h(t) \equiv \int_{-\infty}^{t} dt'\, x(t')\, h(t-t') \tag{17}$$

The TDFRS experiments discussed are performed with periodic boundary conditions, asking for the discrete periodic convolution

$$y[n] = x[n] * h[n] \equiv \sum_{i=0}^{N-1} x[i]\, h[(n-i) \bmod N] \tag{18}$$

The convolution theorem turns Eqs. (17) and (18) into simple products in frequency space:

$$Y = XH \tag{19}$$

The discrete periodic correlation is defined in analogy as

$$y[n] = x[n] \times h[n] \equiv \sum_{i=0}^{N-1} x[i]\, h[(n+i) \bmod N] \tag{20}$$

$$Y = X^* H \tag{21}$$

X^* is the complex conjugate of X. No arguments are used in Eqs. (19) and (21) since they apply to both the continuous and discrete cases.

From Eqs. (19) and (21), it is immediately evident that h is obtained from the deconvolution

$$H = \frac{Y}{X} = \frac{YX^*}{|X|^2} \tag{22}$$

followed by the transition to the time domain according to Eq. (12). From the right-hand side of Eq. (22) it follows that h may also be determined by cross correlation of the sample response y with the excitation x in case of a white power spectrum with $|X|^2 = 1$.

2.2.2. Definition of the Response Function

Before Eq. (22) can be applied to the experimental problem, the signal flow in the experiment must be considered in detail to identify the proper response function, the corrections that must be applied, and the errors inferred by discrete sampling of the continuous signals. The signal flow is summarized in Fig. 2, and a suitable mapping between the signals in the figure and the actual physical quantities is the following:

A discrete binary sequence $x[n]$ of 1 and -1, defined at times $n\,\Delta t$, $n = 0, 1, \ldots, N-1$, is generated within the computer memory and converted to a continuous binary voltage signal $x(t)$, which drives the high-voltage generator for the Pockels cell. The resulting amplitude of the optical interference grating, $x'(t) \equiv I_q(t)/I_0$, excites the sample, which, in principle, could be described by a single response function $h'(t) = g_T(t) * g(t)$. $h'(t)$ is the convolution of the heat and the concentration modes as indicated by the dashed bracket in Fig. 2.

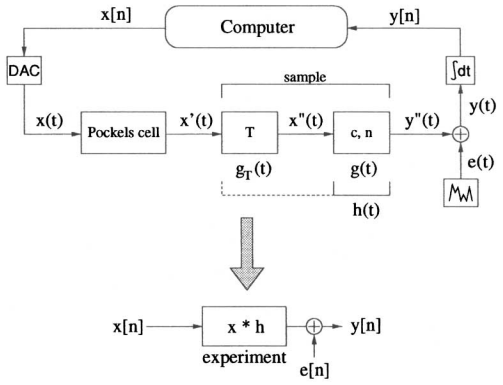

Fig. 2. Sketch of the signal generation. See text for details.

Due to the time scale separation of three to four decades between both modes, it is, however, more convenient to focus on the response of the concentration mode and convolute the heat mode $g_T(t) = \tau_{th}^{-1} \exp(-t/\tau_{th})$ into the effective excitation, hence,

$$x''(t) = T_q(t) \left[\frac{\alpha}{\rho c_p} I_0 \tau_{th} \right]^{-1} \tag{23}$$

$T_q(t)$ is given in Eqs. (3) and (4).

Now, the effective linear response function $h(t)$ can be identified with $g(t)$ as defined in Eqs. (9) and (10): $h(t) \equiv g(t)$. It contains both the response of the concentration mode and the infinitely fast translation of the concentration and the driving temperature grating into the measurable heterodyne diffraction efficiency $y''(t) \equiv \zeta_{het}(t)$. The instantaneous contribution of the temperature grating to the diffraction efficiency is expressed by the δ-function in $g(t)$. After the sample, an unavoidable noise term $e(t)$ is added. The continuous signal $y(t)$ is sampled by integrating with an ideal detector over time intervals Δt to obtain the time discrete sequence $y[n]$ for processing in the computer.

There are several reasons why we focus on $g(t)$ and not the entire response function of the sample, $g_T(t) * g(t)$. The first one is trivial, since our main interest is not heat transport but mass and thermal diffusion in polymeric systems. Furthermore, experience shows that in a typical experiment with long step-like excitations the measured amplitudes from both modes are approximately equal. Since these saturation amplitudes are proportional to the respective time constants τ_{th} and τ, it is straightforward to show that this translates into a difficult-to-handle amplitude ratio of up to 10^4 between the fast heat and the slow concentration mode in the total response function $g_T(t) * g(t)$. By convoluting $g_T(t)$ into the excitation and employing sample times $\tau_{th} \ll \Delta t \ll \tau$ the disparity between both signal amplitudes reduces to a much more convenient $O(\tau/\Delta t)$.

In summary, the TDFRS experiment converts an ideal time discrete excitation $x[n]$ into a time discrete signal $y[n]$, involving both linear and nonlinear components like the sample itself or the Pockels cell. The task is to extract the response $h(t) \equiv g(t)$ from $y[n]$ when $x[n]$ is known. This idealized view of the experiment is shown in the lower part of Fig. 2. All the missing components from the upper part of Fig. 2 are treated as perturbations, which can be accounted for in a well conducted experiment.

2.3. Selection of the Excitation Pattern

So far not much has been said about the excitation sequence $x[n]$ except that the considerations will be restricted to binary sequences of

amplitude $+1$ and -1, corresponding to 180° phase jumps of the holographic intensity grating at maximum modulation depth. Such binary sequences combine the advantage of high spectral power density for linear heterodyne detection with easy experimental handling.

2.3.1. Noise Amplification

The total power P in the excitation is obtained from Parseval's theorem:

$$P = \sum_{k=0}^{N-1} |X[k]|^2 = N \sum_{n=0}^{N-1} x[n]^2 \tag{24}$$

Since the power at zero frequency, $|X[0]|^2$, merely adds a constant background without much information content, the requirement for maximum excitation power P_+ at positive frequencies is

$$\begin{aligned} P_+ = \sum_{k=1}^{N-1} |X[k]|^2 &= N \sum_{n=0}^{N-1} x[n]^2 - \left(\sum_{n=0}^{N-1} x[n] \right)^2 \\ &= N^2(\langle x^2 \rangle - \langle x \rangle^2) \end{aligned} \tag{25}$$

P_+ reaches a maximum for $\langle x \rangle = 0$. Hence, an excitation sequence should contain, at least, approximately the same number of $+1$ and -1.

Further constraints are imposed by the unavoidable noise term $e[n]$, which adds to the signal:

$$Y = XH + E \tag{26}$$

The arguments are omitted, and the frequency domain notation has been chosen for simplicity. After deconvolution the experimentally determined memory function contains the true memory function plus an error term:

$$\frac{YX^*}{|X|^2} = H + E \frac{X^*}{|X|^2} \tag{27}$$

From Eq. (27) the amplification U_k of the spectral power density of the noise is

$$U_k = \left| \frac{X^*[k]}{|X[k]|^2} \right|^2 = |X[k]|^{-2} \tag{28}$$

and the integral noise amplification

$$U = \sum_{k=0}^{N-1} |X[k]|^{-2} \tag{29}$$

U is minimized for a constant white power spectrum with $|X[k]|^2 = N$ according to Eq. (24), yielding $U = 1$. All deviations from the constant power spectrum increase the integral noise amplification U. They may, however, be employed for noise suppression at selected frequencies.

Arbitrary random binary sequences generally have a globally flat power spectrum but a high noise amplification due to a locally rugged structure of the spectral power density with large values of U_k. Efficient excitation sequences can be generated from random binary sequences by successive optimization. This problem is equivalent to the one of minimizing the energy of an Ising spin system, where the spins are represented by the excitation pulses ($+1$ or -1) and the energy U is defined in Eq. (29). With simple one-spin-flip optimization, where subsequently all spins are tested and flipped only if the energy is reduced, $U \approx 1.15$ is easily achieved. More sophisticated techniques, like simulated annealing, give only slight improvements [13]. For practical purposes such optimized sequences are almost ideal. As an example, optimization reduces the noise amplification of a particular but arbitrarily chosen random binary sequence of length $N = 2^{12}$ from $U = 17.3$ to $U = 1.18$, which is almost identical to the theoretical limit $U = 1$ for all practical purposes.

Another class of suitable excitations with a perfectly white power spectrum includes maximum length binary sequences (MLBS) of length $N = 2^L - 1$, L being a positive integer [10]. MLBS have been employed in Hadamard NMR spectroscopy [11], and the deconvolution according to Eq. (22) is efficiently computed by means of a fast Hadamard transform. The performance of MLBS in TDFRS is approximately the same as the one of optimized random sequences. Some peculiarities have been found for MLBS with respect to systematic distortions introduced by the Pockels cell [14]. The computational effort for MLBS of length $N = 2^L - 1$ and sequences of length 2^L is comparable when fast finite Fourier transform algorithms are used.

2.4. Corrections and Limitations

The parts of the experiment that have been omitted when using the simplified description according to Fig. 2 necessitate some corrections and impose limitations that are briefly discussed in the following.

Figure 3 gives a closer look of the measurement process for a hypothetical sample, for simplicity without dissolved polymer. The binary sequence $x[n] = [-1, -1, 1, 1, 1, -1, -1, \ldots]$ is defined at times $t = n\,\Delta t$ and converted to the continuous excitation $x(t)$, which keeps the value $x[n]$ from $t = n\,\Delta t$ until $t = (n+1)\,\Delta t$ as indicated by the dashed line in Fig. 3a.

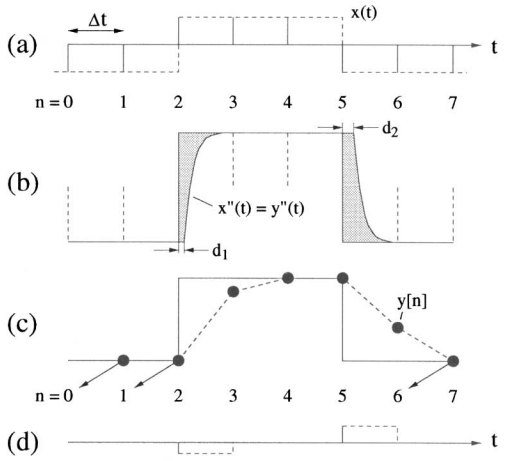

Fig. 3. Details of the measurement: (a) ideal excitation, (b) amplitude of the temperature grating and of the heterodyne signal for $c = 0$, (c) effect of sampling for $y(t) \rightarrow y[n]$, and (d) fictive correction to the ideal excitation.

The temperature grating $x''(t)$ (Fig. 3b) does not follow $x(t)$ instantaneously because of its finite time constant $\tau_{th} \ll \Delta t$ and because there is a delay of several μs caused by the high voltage driver for the Pockels cell, which is asymmetric with respect to the switching direction (d_1 and d_2). As a consequence, everytime the excitation changes its sign, there is some intensity missing in the excitation as shown by the shaded areas.

Sampling is done by integration from $t = n\,\Delta t$ to $t = (n+1)\,\Delta t$, and the result is stored in $y[n]$ (Fig. 3c). To interprete the data as the average over the respective interval, the time scale for $g(t)$ is shifted by $\Delta t/2$ towards higher values.

In the example, the effect of the missing area manifests itself for $y[2]$ and $y[5]$. The finite temperature response and the delay can approximately be accounted for by adding a fictive excitation x_f proportional to the derivative of the ideal excitation to $x[n]$. The asymmetry $d_1 - d_2$ is incorporated in an analogous way, hence

$$x_f[n] = a(x[n] - x[n-1]) + b(x[n] - x[n-1])(1 - x[n-1]) \qquad (30)$$

$x_f[n]$ and $x_f(t)$ are shown in Fig. 3d. a and b are constants and can be determined from separate measurements of the Pockels cell response and τ_{th}. In the language of digital signal analysis, a is due to aliasing of signal

intensity with frequencies above the Nyquist frequency $\omega_{Ny} = \pi/\Delta t$, which are folded back into the frequency interval $-\omega_{Ny} < \omega_k < \omega_{Ny}$. $a = 0$ may be used for simplicity, in which case the thermal amplitude is spread over a few data points instead of being confined to the first one according to the δ-function in Eq. (9). The area is, however, preserved. To avoid signal distortion due to aliasing of the interesting mass diffusion part of the spectrum, the sampling time should, as a rule of thumb, fulfil $\Delta t \leqslant \tau/10$ for the fastest concentration mode. On the other hand, Δt should not be shorter than necessary, since the signal-to-noise ratio can be shown to be proportional to $N^{1/2}\,\Delta t$. This is an improvement by a factor of $N^{1/2}$ over single pulse δ-excitations with pulse length Δt.

3. EXPERIMENT

The setup is almost identical to that used for previous experiments. An argon ion laser (488 nm) is used for writing and a helium–neon laser (633 nm) for reading. Switching of the grating is accomplished by 180° phase shifts by means of a Pockels cell in one of the writing beams such that $+1$ in the excitation sequence corresponds to a phase of 0° and -1 to 180°. A reference wave is provided by scratches or dust on the sample, serving as local oscillator. The phase between the reference and the signal beams is adjusted by means of a piezo-mirror. A PMT in photon counting mode is used for detection. A custom made plug-in card in a PC is used for photon counting and also controls the timing and synchronization between the excitation sequence and the measured PMT signal. The measurements are done in bursts of several repetitions of the excitation sequence $x[n]$, where the first N data points are discarded. Since the system memory is much shorter than $N\,\Delta t$, truly periodic boundary conditions are achieved.

All experiments were conducted in heterodyne mode, and the TDFRS setup and the separation of homodyne and heterodyne signal components have been described in detail in Ref. 7. The solutions are slightly colored with quinizarin to adjust the optical density to 0.02 at the writing wavelength. The path length of the optical cell is 200 μm. All measurements have been performed at room temperature.

4. RESULTS

Figure 4 shows an experiment on almost monodisperse polystyrene (PS; $M \approx 250{,}000$ g·mol^{-1}) in toluene at a concentration of $c = 0.0205$. The scattering vector $q = 9213$ cm^{-1} is well within the hydrodynamic limit $qR_g \ll 1$, where the pure center of mass diffusion is observed. R_g is the

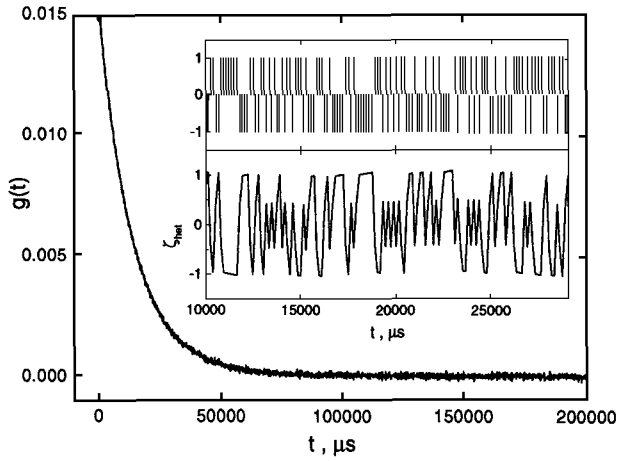

Fig. 4. Memory function $g(t)$ as obtained from an optimized random binary sequence with $N = 2048$. The inset shows a section of the excitation sequence and the corresponding measured heterodyne sample response.

radius of gyration of the polymer. The upper part of the inset is a section of the pulse train of the optimized random binary sequence of length $N = 2^{11}$ used for excitation with a time resolution of $\Delta t = 140\ \mu s$. The lower part of the inset represents the normalized heterodyne diffraction efficiency. The main portion of Fig. 4 shows the concentration part of the memory function $g(t)$ as obtained by deconvolution. For the diffusion time constant $\tau = 13900\ \mu s$, $D = 5.5 \times 10^{-7}\ cm^2 \cdot s^{-1}$ has been found.

The amplitude of the temperature signal in $g(t)$ is normalized to unity and not plotted in Fig. 4. Due to aliasing, it is spread over the first three data points.

A comparison between TDFRS and PCS for a solution of a bimodal molar mass distribution is shown in Fig. 5. The sample is a mixture of two PS with 895 and 250,000 $g \cdot mol^{-1}$ and a dispersity of $M_w/M_n \approx 1.03$ in toluene at concentrations of 0.0166 and 0.00228, respectively.

The heterodyne decay functions for a TDFRS experiment with pseudo-stochastic noise excitation and for a TDFRS experiment with step-excitation are plotted together with the electric field autocorrelation function from PCS in the upper half of Fig. 5. The PCS experiment has been performed at an angle of 90° and a wavelength of 647 nm and the time scale has been shifted according to $\tau \propto q^{-2}$. The TDFRS parameters are $\Delta t = 140\ \mu s$ and $N = 2047$. Blocks of 16 repetitions of the excitation sequence have been accumulated between phase stabilizations for heterodyne detection, and the

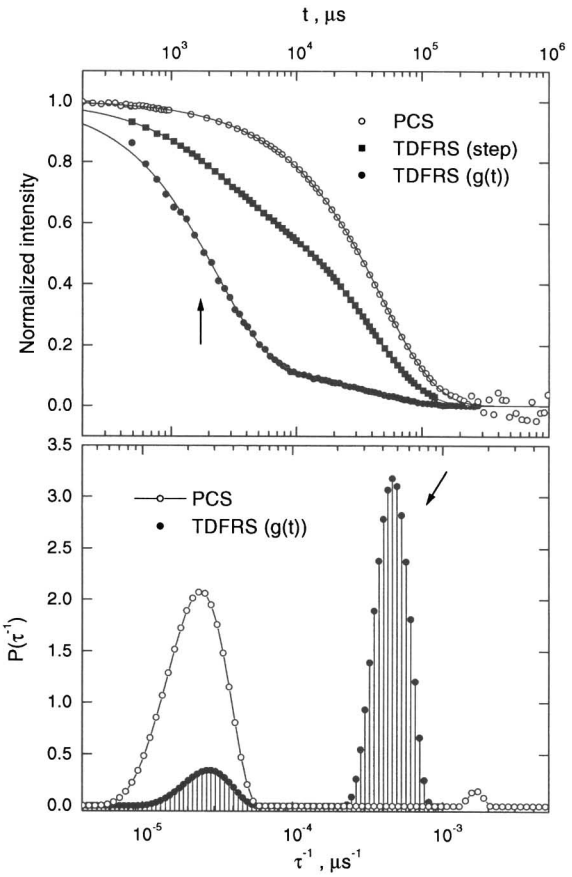

Fig. 5. Comparative measurement of bimodal PS in toluene with PCS and TDFRS with optimized random binary sequence and with step excitation: decay functions (upper) and rate distributions (lower). The fast mode of the light component (895 $g \cdot mol^{-1}$) is marked by arrows.

signal has been averaged over 488 such blocks. The same overall time has been used for all three experiments. The solid lines are biexponential least-squares fits. Both modes are clearly visible in the TDFRS measurements, whereas the PCS correlation function is completely dominated by the slow mode of the high molar mass, despite the seven-fold higher concentration of the low molar mass component. In a PCS experiment on the low molar mass component alone, no diffusion process that exceeded the baseline noise could be observed.

The lower half of Fig. 5 shows the rate distributions for TDFRS with pseudostochastic noise excitation and for PCS as obtained from an inverse Laplace transform using CONTIN [15]. Again, both components are clearly resolved by TDFRS. The PCS rate distribution shows only a large peak for the slow mode. The tiny peak at $\tau^{-1} \approx 1.7 \times 10^{-3}\ \mathrm{s}^{-1}$ is probably an artifact, since its rate is too high when compared with the well resolved TDFRS. The amplitude ratio obtained from the rate distribution for $g(t)$ is 6.8, which is reasonably close to the one expected from the polymer concentrations and the refractive index increments: $[c_1(\partial n/\partial c_1)_{p,T}] \times [c_2(\partial n/\partial c_2)_{p,T}]^{-1} = 5.9$. For the refractive index increments the zero concentration values (0.0736 and 0.0907) of the respective molar mass polymers (895 and 250,000 $\mathrm{g \cdot mol^{-1}}$) have been determined using an interferometric refractometer [16]. The molar mass dependence of $(\partial n/\partial c)_{p,T}$ is due to end group effects of the short chains. From $g(t)$ the thermal diffusion coefficient is calculated according to Eqs. (10) and (11) as $D_T = 1.12 \times 10^{-7}\ \mathrm{cm^2 \cdot s^{-1} \cdot K^{-1}}$, which is in excellent agreement with results found previously in the same laboratory [6].

Figure 6 shows the diffusion susceptibility, which has directly been obtained from the measurement as the Fourier transform of $g(t)$ from Fig. 5, plotted as $|G(\omega)|^2$. The solid lines are least squares fits of the two Lorentzians corresponding to the two approximately exponential modes in $g(t)$:

$$|G(\omega)|^2 = \left| \frac{a_1 \tau_1}{1 + i\omega\tau_1} + \frac{a_2 \tau_2}{1 + i\omega\tau_2} \right|^2 \tag{31}$$

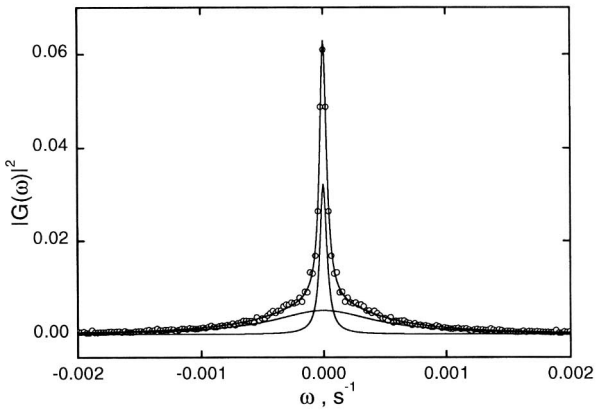

Fig. 6. Diffusion susceptibility $|G(\omega)|^2$ as obtained from the measurement of $g(t)$ in Fig. 5 with the least-squares fit of two Lorentzians, which are also plotted separately.

5. SUMMARY AND CONCLUSION

Signal generation in heterodyne TDFRS can be formulated in the language of linear response theory. For the measurement of diffusion processes it is advantageous to focus on the concentration modes and to lump the temperature response into the excitation. Especially for dilute polymer solutions the response function $g(t)$ of the concentration modes shows interesting properties such as concentration proportional amplitudes of the individual molar mass components. While, due to the poor signal-to-noise ratio, a straightforward measurement of $g(t)$ as response to a δ-excitation is not feasible, pseudostochastic random binary sequences provide an elegant and efficient access to $g(t)$.

For a correct interpretation of the experiment, various corrections and limitations must be considered to avoid problems from, e.g., aliasing. Perfectly white power spectra are realized with MLBS. Optimized random binary sequences offer almost the same noise amplification and the additional opportunity of coloring the excitation spectrum by shifting energy into interesting frequency ranges. A detailed discussion of colored spectra is, however, beyond the scope of this paper.

Besides the direct measurement of the linear response function, pseudostochastic random binary sequences provide additional advantages such as time-scale delocalization and frequency multiplexing. As a consequence of time-scale delocalization, a singular perturbation from, e.g., dust particles does not deform the decay function locally but is spread over the entire time axis as random noise. Frequency multiplexing drastically reduces the stability requirement for experiments in the frequency domain in order to obtain the diffusion susceptibility $G(\omega)$. If all frequencies were measured subsequently, stability over the whole duration of the experiment would be required, whereas frequency multiplexing reduces the stability requirement to several excitation periods $N\,\Delta t$.

From a well-conducted experiment, precise values for the transport coefficients are obtained, as has been demonstrated for a bimodal PS mixture. For this polydisperse sample both components are resolved and the low molar mass component has been recovered with a large concentration proportional amplitude, whereas the PCS correlation function is dominated entirely by the heavy component.

A critical assessment of the experimental errors and the achievable accuracies of the transport coefficients is by no means a trivial task. Potential sources of error, such as excessive sample heating and convection, and the achievable signal-to-noise ratio as a function of the experimental parameters, have been discussed in detail in Ref. 7 for TDFRS with long exposure pulses. In principle, similar arguments apply to stochastic

TDFRS, with the difference that low-molar mass components are not masked by the presence of relatively little high-molar-mass material. Unfortunately, there are also new sources of error, that stem from imperfections in the switching behavior. These errors accumulate because of the large number of 180° phase switches in stochastic TDFRS. Under favorable conditions, we estimate the achievable accuracy to be approximately 1% for both D and D_T. In case of polydisperse samples, the same accuracy can be achieved for the average diffusion coefficient $\langle D \rangle$, but the individual modes in a broad rate distribution are certainly less precise. Clearly, accurate values for D and D_T require the precise knowledge of the refractive index increments [16] and of the grating vector q.

ACKNOWLEDGMENTS

The authors thank C. Rosenauer for the PCS measurements and B. Müller for the measurement of the refractive index increments.

REFERENCES

1. K. Thyagarajan and P. Lallemand, *Opt. Commun.* **26**:54 (1978).
2. F. Bloisi, L. Vicari, P. Cavaliere, S. Martellucci, J. Quartieri, P. Mormile, and G. Pierattini, *Appl. Phys.* **B44**:103 (1987).
3. W. Köhler, *J. Chem. Phys.* **98**:660 (1993).
4. F. Bloisi, *Opt. Commun.* **68**:87 (1988).
5. P. Rossmanith and W. Köhler, *Macromolecules* **29**:3203 (1996)
6. W. Köhler, C. Rosenauer, and P. Rossmanith, *Int. J. Thermophys.* **16**:11 (1995).
7. W. Köhler and P. Rossmanith, *J. Phys. Chem.* **99**:5838 (1995).
8. W. Köhler and B. Müller, *J. Chem. Phys.* **103**:4367 (1995).
9. M. E. Schimpf and J. C. Giddings, *J. Polym. Sci. Polym. Phys.* **B27**:1317 (1989).
10. D. Ziessow, *On-line Rechner in der Chemie* (de Gruyter, Berlin, 1973).
11. D. Ziessow and B. Blümich, *Ber. Bunsenges. Phys. Chem.* **78**:1168 (1974).
12. S. D. Stearns, *Digitale Verarbeitung analoger Signale* (Oldenburg, München, 1987).
13. W. Köhler and R. Schäfer, in press (1997).
14. R. Schäfer, Ph.D. thesis (Johannes-Gutenberg Universität, Mainz, 1997).
15. S. W. Provencher, *Comput. Phys. Commun.* **27**:229 (1982).
16. A. Becker, W. Köhler, and B. Müller, *Ber. Bunsenges. Phys. Chem.* **99**:600 (1995).